


## Impact of tensor forces on spin-orbit splittings in neutron-proton drops

Qiang Zhao (赵强) <sup>1</sup>, Pengwei Zhao (赵鹏巍)<sup>1</sup>, and Jie Meng (孟杰)<sup>1,2,3,\*</sup>

<sup>1</sup>State Key Laboratory of Nuclear Physics and Technology, School of Physics, Peking University, Beijing 100871, China

<sup>2</sup>School of Physics and Nuclear Energy Engineering, Beihang University, Beijing 100191, China

<sup>3</sup>Yukawa Institute for Theoretical Physics, Kyoto University, Kyoto 606-8502, Japan



(Received 7 May 2020; revised 24 July 2020; accepted 3 September 2020; published 18 September 2020)

A systematic study of the tensor-force impact in neutron-proton drops has been reported using the relativistic Hartree-Fock (RHF) theory with the  $\pi$ - $N$  coupling strength optimized to the relativistic Brueckner-Hartree-Fock (RBHF) results for neutron drops. The evolutions of the neutron spin-orbit splittings as a function of the neutron number for neutron-proton drops with one proton behave similarly to the pure neutron drops, which show the tensor-force effect. By adding one more proton or neutron in the neutron drop with  $N = 20$ , it is found that the tensor-force effect is more prominent between neutrons and protons than between neutrons. This can be attributed to the isospin factor in the tensor term of the  $\pi$ - $N$  interaction in the RHF density functional theory, which reflects the fact that the neutron-proton tensor force is stronger than the neutron-neutron one. Similar behavior for the spin-orbit splitting evolutions has also been found for the neutron-proton drops with 20 protons, where the tensor-force strength  $\lambda$  is redetermined according to the RBHF results due to the large central densities of the systems.

DOI: [10.1103/PhysRevC.102.034322](https://doi.org/10.1103/PhysRevC.102.034322)

### I. INTRODUCTION

Tensor force is one of the important topics in nuclear physics [1–3]. As an important ingredient of the nuclear force, it is responsible for the electric quadrupole moment of the deuteron [4] and the binding of light nuclei [5–8]. It also plays an essential role in explaining the shell evolution in exotic nuclei far away from the stability line [9], which is associated with the emergence of new magic numbers and the disappearance of the traditional ones. In addition, the tensor-force effects are also found to be important for the description of spin-isospin excitations [10,11]. Therefore, a lot of efforts have been made to study the tensor-force effects in the non-relativistic and relativistic density functional theories (DFTs).

Many successes in nuclear physics have been achieved with the nuclear covariant density functional theory (CDFT) [12]. It is well-known that the tensor force comes mainly from the exchange of  $\pi$  mesons. However, the  $\pi$  mesons are neglected in most widely used covariant density functionals because they do not contribute on the Hartree level, except for the nonlocal functionals with Fock terms in the framework of the relativistic Hartree-Fock (RHF) theory [13,14]. In the RHF framework, the tensor-force effects in other meson-nucleon coupling channels have also been studied [15–17]. It is found that with the  $\pi$ -exchange and  $\rho$ -tensor couplings, the RHF functionals could improve the description of the single-particle energies for finite nuclei [18–22].

Nevertheless, the determination of the strength of the tensor force is still a challenging problem. On the one hand,

the density functionals are usually determined by fitting to the bulk properties of nuclear matter and finite nuclei, which are not sensitive to tensor force. In fact, it has been found that an optimal fit for the binding energies and the charge radii is achieved with a vanishing  $\pi$ -meson field [23]. On the other hand, though the single-particle energy is believed to be sensitive to the tensor forces, it is also influenced considerably by the beyond mean-field effects [24,25], e.g., the particle-vibration couplings. Because it is difficult to find significant features in experimental data that are only connected to tensor forces, much attention has been paid to the metadata from microscopic *ab initio* calculations for constraining the strength of tensor forces.

A neutron drop provides an ideal platform to link the calculated results with *ab initio* approaches and DFTs [2,3,26–30]. It contains a certain number of neutrons, which are confined in an external field. Because only the neutron-neutron interactions exist in neutron drops, they can be calculated with both *ab initio* methods [26,27,31–37] and DFTs [28–30]. So far, many properties of neutron drops including the binding energies, radii, and spin-orbit (SO) splittings have been studied with different approaches. In Ref. [29], the radii of neutron drops have even been linked to experimental neutron skin thicknesses of finite nuclei with strong linear correlations, which in turn can be used to constrain the three-neutron forces.

As for the tensor-force effects in neutron drops, it has been found from the fully self-consistent relativistic Brueckner-Hartree-Fock (RBHF) calculations [38,39] that the evolution of SO splittings along with the increasing neutron number in neutron drops exhibits a significant tensor-force effect [2]. Moreover, a recent study has shown that the strength of the

\* mengj@pku.edu.cn

tensor forces in DFTs runs with the strength of the external fields of neutron drops to reproduce the RBHF SO splittings, due to the density dependence of the density functionals [40].

In all these studies for neutron drops, however, the tensor forces are only among neutrons, and the information for the neutron-proton tensor forces is missing. In Ref. [41], two neutron-proton drops  $^{40}\text{20}$  and  $^{48}\text{20}$ , which are confined in harmonic oscillator fields, are calculated with the RBHF theory, and the obtained results have been used to constrain the Skyrme density functional.

Because the RBHF results for the SO splittings in the neutron drops can be well reproduced with the RHF density functional PKO1 [14] by adjusting the  $\pi$  coupling, in this work, a systematic study of the impact of tensor forces in neutron-proton drops is presented with the RHF functional PKO1, where the  $\pi$  coupling strength is optimized to the RBHF results for neutron drops.

This paper is organized as follows. In Sec. II, a brief introduction to the RHF theory is provided, and the calculated results and the discussions for the SO splittings in neutron-proton drops are presented in Sec. III. Finally, the summary is given in Sec. IV.

## II. THEORETICAL FRAMEWORK

In the CDFT, the nucleon-nucleon interaction is mediated by the exchange of mesons. The Hamiltonian  $H$  of a nuclear many-body system is written as

$$H = \sum_{\alpha\beta} T_{\alpha\beta} c_{\alpha}^{\dagger} c_{\beta} + \frac{1}{2} \sum_{\alpha'\beta'\alpha''\beta''} V_{\alpha'\beta'\alpha''\beta''}^{\phi} c_{\alpha'}^{\dagger} c_{\beta'}^{\dagger} c_{\beta''} c_{\alpha''}. \quad (1)$$

$T_{\alpha\beta}$  is the kinetic term and  $V_{\alpha'\beta'\alpha''\beta''}^{\phi}$  is the two-body interaction described by the exchange of mesons and photons:

$$\begin{aligned} T_{\alpha\beta} &= \int d\mathbf{r} \bar{\psi}_{\alpha}(\mathbf{r})(-i\boldsymbol{\gamma} \cdot \nabla + M)\psi_{\beta}(\mathbf{r}), \\ V_{\alpha'\beta'\alpha''\beta''}^{\phi} &= \iint d\mathbf{r}_1 d\mathbf{r}_2 \bar{\psi}_{\alpha'}(\mathbf{r}_1) \bar{\psi}_{\beta'}(\mathbf{r}_2) \Gamma_{\phi}(\mathbf{r}_1, \mathbf{r}_2) \\ &\quad \times D_{\phi}(\mathbf{r}_1, \mathbf{r}_2) \psi_{\beta''}(\mathbf{r}_2) \psi_{\alpha''}(\mathbf{r}_1). \end{aligned} \quad (2)$$

$\psi_{\alpha}(\mathbf{r})$  is the Dirac spinor for nucleons. The index  $\phi$  runs over different types of meson and photon fields, and  $\Gamma_{\phi}(\mathbf{r}_1, \mathbf{r}_2)$  and  $D_{\phi}(\mathbf{r}_1, \mathbf{r}_2)$  represent the interaction vertex and propagator, respectively. The indices  $\alpha, \beta, \alpha',$  and  $\beta'$  run over all the positive single-particle states  $\{\psi_{\alpha}\}$  under the no-sea approximation.

The energy functional  $E$  can be obtained as the expectation value of the Hamiltonian on the Hartree-Fock ground state  $|\Phi_0\rangle$ ,

$$E = \langle \Phi_0 | H | \Phi_0 \rangle. \quad (3)$$

Assuming spherical symmetry, the variation of the energy functional with respect to the Dirac spinor gives the relativistic Hartree-Fock equation as

$$\int d\mathbf{r}' h(\mathbf{r}, \mathbf{r}') \psi(\mathbf{r}') = \varepsilon \psi(\mathbf{r}). \quad (4)$$

Here,  $\varepsilon$  is the single-particle energy. The single-particle Dirac Hamiltonian  $h(\mathbf{r}, \mathbf{r}')$  contains the kinetic part  $h^{\text{kin}}$ , the direct

potential  $h^{\text{D}}$ , and the exchange potential  $h^{\text{E}}$  with the expressions

$$h^{\text{kin}}(\mathbf{r}, \mathbf{r}') = [\boldsymbol{\alpha} \cdot \mathbf{p} + \beta M] \delta(\mathbf{r} - \mathbf{r}'), \quad (5a)$$

$$h^{\text{D}}(\mathbf{r}, \mathbf{r}') = [\beta \Sigma_S(\mathbf{r}) + \Sigma_0(\mathbf{r}) + U_{\text{ex}}(\mathbf{r})] \delta(\mathbf{r} - \mathbf{r}'), \quad (5b)$$

$$h^{\text{E}}(\mathbf{r}, \mathbf{r}') = \begin{pmatrix} Y_G(\mathbf{r}, \mathbf{r}') & Y_F(\mathbf{r}, \mathbf{r}') \\ X_G(\mathbf{r}, \mathbf{r}') & X_F(\mathbf{r}, \mathbf{r}') \end{pmatrix}. \quad (5c)$$

The local self-energies  $\Sigma_0$  and  $\Sigma_S$  come from the contributions of the direct terms, and the nonlocal ones  $X_G, X_F, Y_G,$  and  $Y_F$  are given by the exchange terms. More details can be found in Refs. [13,14,42]. For neutron and neutron-proton drops, the external field  $U_{\text{ex}} = \frac{1}{2} M \omega^2 r^2$  is included in the single-particle Dirac Hamiltonian.

For the  $\pi$ -exchange potential, the two-body interaction  $V^{\pi}$  can be expressed in the momentum space as

$$V^{\pi}(\mathbf{q}) = -\frac{1}{3} \left( \frac{f_{\pi}}{m_{\pi}} \right)^2 \frac{1}{m_{\pi}^2 + \mathbf{q}^2} [S_{12} + \boldsymbol{\sigma}_1 \cdot \boldsymbol{\sigma}_2 \mathbf{q}^2] \vec{\tau}_1 \cdot \vec{\tau}_2, \quad (6)$$

where the tensor-force operator reads

$$S_{12}(\mathbf{q}) \equiv 3(\boldsymbol{\sigma}_1 \cdot \mathbf{q})(\boldsymbol{\sigma}_2 \cdot \mathbf{q}) - \boldsymbol{\sigma}_1 \cdot \boldsymbol{\sigma}_2 \mathbf{q}^2 \quad (7)$$

and  $\mathbf{q}$  denotes the exchange momentum between two nucleons. The coupling constant  $f_{\pi}$  is assumed to be density-dependent,

$$f_{\pi}(\rho) = f_{\pi}(0) e^{-a_{\pi} \rho}, \quad x = \rho / \rho_{\text{sat}}, \quad (8)$$

where  $\rho$  is the baryonic density and  $\rho_{\text{sat}}$  is the saturation density of symmetric nuclear matter. The density dependence is determined by the parameter  $a_{\pi}$ . In this work, as in Refs. [2,40], the coupling constant  $f_{\pi}$  is multiplied with a factor  $\lambda$  to simulate the strength of the tensor force in RBHF calculations. Note that the  $\rho$ -tensor coupling is not considered explicitly in the functional PKO1, and its contribution to the tensor-force effects is effectively included in the  $\pi$  meson by adjusting the coupling strength.

## III. RESULTS AND DISCUSSION

Similar to neutron drops, the neutron-proton drop is an ideal system, in which the protons and neutrons are confined in an external field, and the Coulomb interaction is neglected. The external field is chosen as the harmonic oscillator potential with the strength  $\hbar\omega = 10$  MeV. We first study the simplest neutron-proton drop, which contains only one proton. It is known from Ref. [40] that the strength of the tensor force depends strongly on the density of the system. However, in this simplest neutron-proton drop, the additional proton does not change the density very much. Therefore, the  $\pi$ - $N$  coupling constant is rescaled with a factor  $\lambda = 1.4$ , which is similar to the one used for pure neutron drops in Refs. [2,40].

In the left panels of Fig. 1, the SO splittings of single-neutron levels are shown as a function of the neutron number  $N$  for the simplest neutron-proton drops with the single proton being placed on either the  $1d_{3/2}$  level or the  $1d_{5/2}$  level. For comparison, the results of pure neutron drops are also presented. The staggering behavior of the SO splittings with the neutron number  $N$  reveals clearly the tensor-force effects.

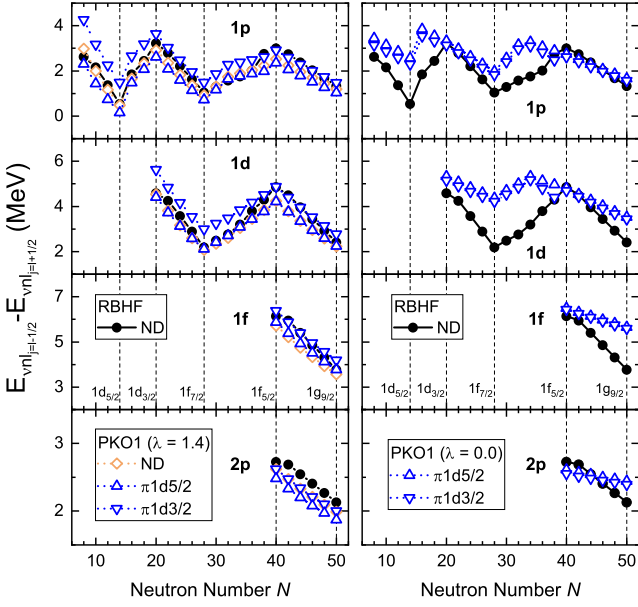


FIG. 1. Spin-orbit splittings of single-neutron states  $1p$ ,  $1d$ ,  $1f$ , and  $2p$  as a function of the neutron number  $N$  for neutron drops and neutron-proton drops with  $Z = 1$ . The single proton in the neutron-proton drops is placed on either the  $1d_{3/2}$  level or the  $1d_{5/2}$  level. For comparison, the relativistic Brueckner-Hartree-Fock results for neutron drops [2] are also presented as solid circles. The RHF functional PKO1 with factor  $\lambda = 1.4$  (left panels) and PKO1 with  $\lambda = 0.0$  (right panels) are used.

With only one proton, the evolution of the neutron SO splittings is very similar to that of the pure neutron drops, due to the fact that the tensor-force between protons and neutrons is not dominated in the neutron-proton drop with  $Z = 1$ . Nevertheless, quantitatively the magnitudes of the splitting energies are changed by the additional proton. In particular, the splittings for the systems with the proton on the  $1d_{3/2}$  level are larger than those for the systems with the proton on the  $1d_{5/2}$  level. This could also be explained by the tensor-force effects; i.e., two single-particle levels with their spins aligned (antialigned) are repulsive (attractive) [9].

In the right panels of Fig. 1, the  $\pi$ -exchange term is neglected by setting  $\lambda$  to zero for neutron-proton drops. The staggering behavior of the SO splittings are much weakened, and the turning points at  $N = 20$  and  $40$  disappear. Placing the single proton on the  $1d_{3/2}$  level or the  $1d_{5/2}$  level does not change the SO splittings significantly, and this is in contrast with the results presented with the tensor force in the  $\pi$ -exchange term.

The influence of the single proton on the neutron SO splittings can be more clearly seen by the differences between the splittings for neutron-proton drops with  $Z = 1$  (ND +  $p$ ) and pure neutron drops (ND). These results are shown in Fig. 2, where for the neutron-proton drops, the single protons are placed on the orbits of  $1p$ ,  $1d$ ,  $1f$ , and  $2p$ , respectively. No matter which orbit the proton is placed on, due to the tensor-force effects, the SO splittings associated with the  $j_> = l + 1/2$  proton are smaller than those with the  $j_< = l - 1/2$  one.

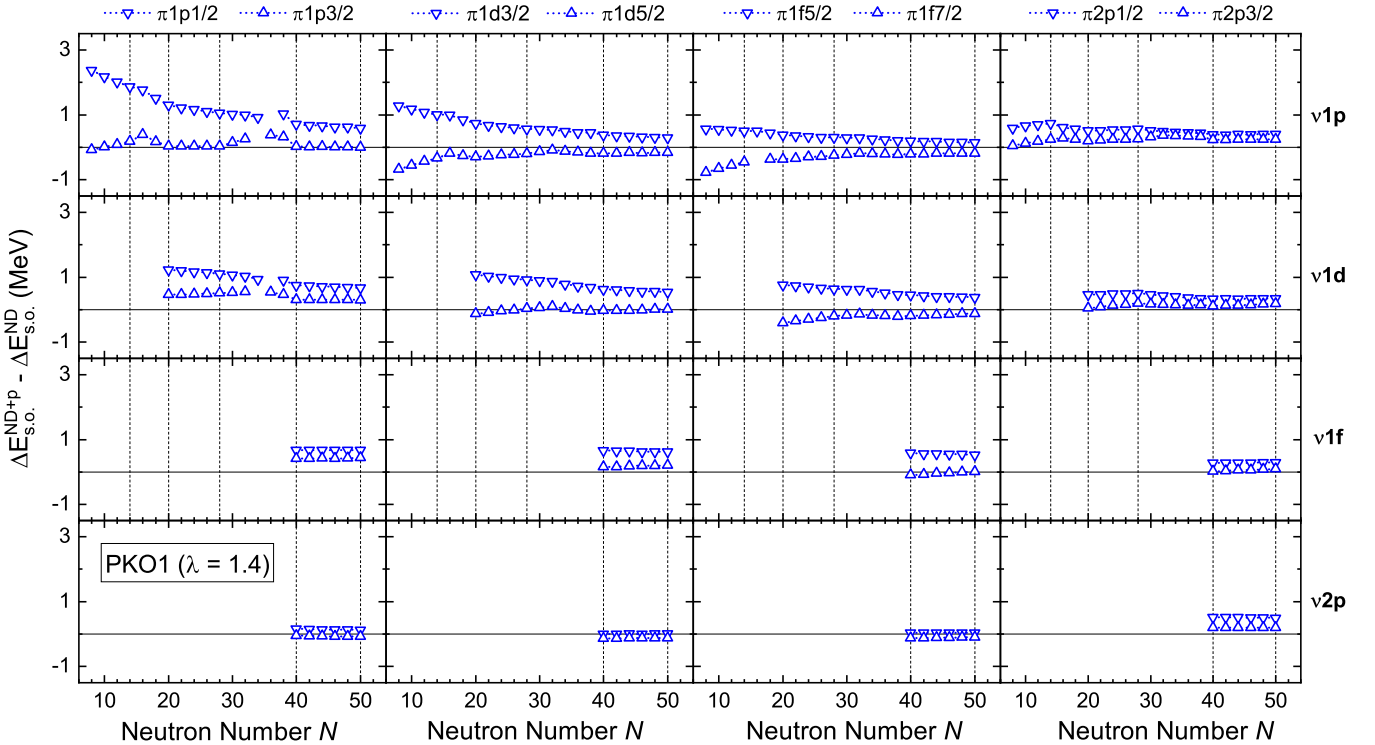


FIG. 2. Differences between the neutron SO splittings for neutron-proton drops with  $Z = 1$  (ND +  $p$ ) and those for pure neutron drops (ND). The up triangles denote the results with the proton placed in the orbits with  $j_> = l + 1/2$  ( $1p_{3/2}$ ,  $1d_{5/2}$ ,  $1f_{7/2}$ , and  $2p_{3/2}$ ), and the down triangles stand for results with the proton placed in the orbits with  $j_< = l - 1/2$  ( $1p_{1/2}$ ,  $1d_{3/2}$ ,  $1f_{5/2}$ , and  $2p_{1/2}$ ). The dashed vertical lines delineate the neutron levels as indicated in Fig. 1.

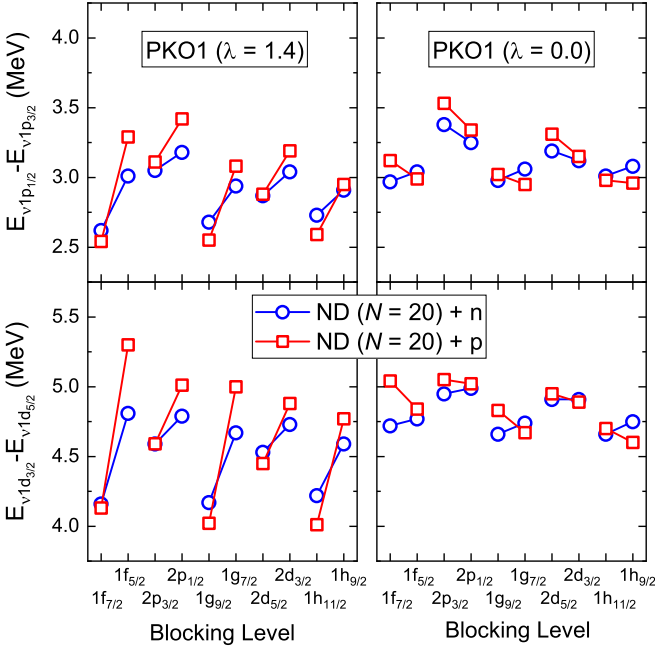


FIG. 3. Spin-orbit splittings of single-neutron states  $1p$  (top) and  $1d$  (bottom) for an ideal drop consisting of 20 neutrons and one more proton or neutron placed in different levels, which are trapped in an external harmonic oscillator trap with  $\hbar\omega = 10$  MeV. The open squares (circles) represent the results with an odd proton (neutron) placed on the orbits  $1f$ ,  $2p$ ,  $1g$ ,  $2d$ , and  $1h$ . The RHF functional PKO1 with factor  $\lambda = 1.4$  (left panels) and PKO1 with  $\lambda = 0.0$  (right panels) are used.

This phenomenon becomes less evident when more neutrons are included in the system, and this is understandable because the tensor force between protons and neutrons becomes less and less dominated with increasing neutron number.

Moreover, one can also see in Fig. 2 that the neutron SO splittings of a given pair of SO states, e.g., the  $1p$  states, are strongly influenced by the single proton on the levels with the same quantum numbers, i.e., the  $1p_{1/2}$  proton or the  $1p_{3/2}$  proton. This is due to the fact that the tensor-force between protons and neutrons has the strongest impact for the states with the same quantum numbers.

To further study the neutron-proton tensor force, one proton or neutron is added in the neutron drop with  $N = 20$  and  $\hbar\omega = 10$  MeV and is placed on different levels ( $1f$ ,  $2p$ ,  $1g$ ,  $2d$ , and  $1h$ ). In the left panels of Fig. 3, the calculated neutron SO splittings of the  $1p$  and  $1d$  orbits are presented. It is clear that the SO splittings for systems with the odd nucleon at the  $j_<$  states are larger than those for systems with the odd nucleon at the  $j_>$  states. This effect cannot be seen any more without the  $\pi$ -exchange term, as shown in the right panels of Fig. 3. Moreover, this effect is more prominent for the systems with an odd proton than those with an odd neutron. Thus, it indicates that the neutron-proton tensor-force effects are stronger than the neutron-neutron ones. This can be attributed to the tensor term in the  $\pi$ - $N$  interaction [see Eq. (6)], where the isospin operator  $\vec{\tau}_1 \cdot \vec{\tau}_2$  provides the Fock terms in the

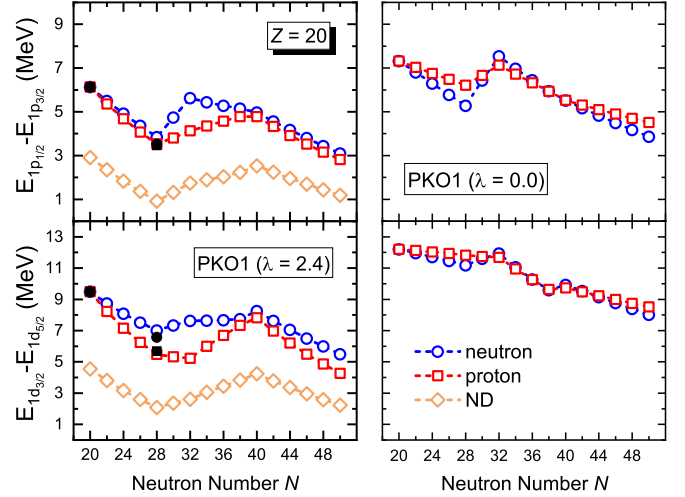


FIG. 4. Spin-orbit splittings of single-particle states  $1p$  (top) and  $1d$  (bottom) in neutron-proton drops ( $Z = 20$ ) as a function of the neutron number  $N$ . The open circles (squares) represent the SO splittings of neutron (proton) levels calculated by the RHF functional PKO1 with  $\lambda = 2.4$  (left panels) and  $\lambda = 0.0$  (right panels). The solid circles (squares) represent the neutron (proton) SO splittings calculated by the RBHF approach [41], and they are renormalized to the RHF results of the drop with 20 neutrons. The RHF results of pure neutron drops in Fig. 1 are also shown for comparison. The strength of the external HO field is taken as  $\hbar\omega = 10$  MeV.

isospin space as

$$\langle q_\alpha | \vec{\tau}_1 | q_\alpha' \rangle \cdot \langle q_\beta | \vec{\tau}_2 | q_\beta' \rangle = (2 - \delta_{q_\alpha, q_\beta}) \delta_{q_\alpha, q_\beta'} \delta_{q_\beta, q_\alpha'} \quad (9)$$

Here,  $q_\alpha$  represents the isospin quantum number of the state  $|\alpha\rangle$ . Therefore, it is clear that the neutron-proton tensor force should be stronger than the neutron-neutron one by a factor of 2, and this is also consistent with the results in the right panels of Fig. 3.

For both  $1p$  and  $1d$  SO splittings, the splitting energy differences between systems with the  $j_<$  odd nucleon and those with the  $j_>$  one are largest when the odd nucleon is placed at the  $1f$  orbits. This is again due to the fact that the tensor force is stronger for two states with similar quantum numbers than those with quite different ones.

Finally, the neutron-proton drops with 20 protons in the external HO field with  $\hbar\omega = 10$  MeV are investigated, and the SO splittings of the single-particle states  $1p$  and  $1d$  are shown in Fig. 4 as a function of the neutron number  $N$ . For comparison, the RHF results for pure neutron drops are also presented. Note that the central densities for the proton-neutron drops with  $Z = 20$  are about two times the saturation density  $\rho_{\text{sat}}$ , while for pure neutron drops the central densities are around  $\rho_{\text{sat}}$ . According to the previous work [40], the optimized tensor-force strength  $\lambda$  in the RHF theory, which reproduces the microscopic RBHF spin-orbit splittings, is running with the central densities of the systems. Therefore, it is apparent that the value of  $\lambda = 1.4$ , which is optimized for pure neutron drops, is no longer appropriate for the present proton-neutron drops with  $Z = 20$ . Accordingly, the factor  $\lambda$  is redetermined by reproducing the differences of the SO splittings at  $N = 20$



and  $N = 28$  for the neutron-proton drops with  $Z = 20$  in the microscopic RBHF results [41], and the resultant value is  $\lambda = 2.4$ . The corresponding RHF results are presented in the right panels of Fig. 4.

The SO splittings of the neutron-proton drops are overall larger than the results for the pure neutron drops. This is due to the fact that the mean potential is deepened by the attractive proton-neutron interactions, which enlarges the SO splittings. Note that the proton and neutron SO splittings are the same for  $N = 20$  and approximately equal for  $N = 40$  because the tensor force should have no influence for spin-saturated systems.

From  $N = 20$  to  $N = 28$ , the neutrons are filling the  $1f_{7/2}$  level. According to the tensor-force impact, the SO splittings for the  $1p$  and  $1d$  levels, as shown in the left panels of Fig. 4, should decline with the increasing neutron number. Similar behavior is also found for the pure neutron drops. Nevertheless, the decrease of the proton SO splittings is greater than the neutron ones, especially for the  $1d$  levels, and this is due to the fact that the neutron-proton tensor force is stronger than the neutron-neutron one.

From  $N = 28$  to  $N = 32$ , the neutrons are filling the  $2p_{3/2}$  level. The SO splittings should, in principle, decrease with the neutron number according to the character of the tensor force. However, because the  $2p_{3/2}$  level has a radial quantum number different from that of the  $1p$  and  $1d$  orbits, the corresponding tensor-force impact is not obvious.

From  $N = 34$  to  $N = 40$ , the neutrons are occupying the  $1f_{5/2}$  and  $2p_{1/2}$  levels. One can see that the proton SO splittings of the  $1p$  and  $1d$  levels rise with the neutron number due to the tensor-force effect. Nevertheless, the evolution of the neutron SO splittings is more flat, or even slightly declines for the  $1p$  orbits. This reflects again that the tensor force between neutrons is not as strong as that between protons and neutrons.

From  $N = 40$  to  $N = 50$ , the neutrons are filling the  $1g_{9/2}$  level and, thus, the tensor force would reduce the SO splittings of the  $1p$  and  $1d$  levels again.

In the right panels of Fig. 4, the calculated results with  $\lambda = 0.0$  are presented. It is found that the staggering of the SO splittings is much influenced by the tensor terms. Particularly, the SO splittings are decreasing from  $N = 32$  to  $N = 40$  without the tensor force. This again reflects that the

tensor force plays an important role in the evolution of the SO splittings.

#### IV. SUMMARY

In summary, the impact of tensor forces in neutron-proton drops has been reported with the RHF functional PKO1, where the  $\pi$  coupling strength is optimized to the RBHF results for neutron drops. The evolution of the neutron spin-orbit splittings as a function of the neutron number for neutron-proton drops with one proton is analyzed by placing the proton on different single-particle levels. Similar to pure neutron drops, the tensor force plays an essential role in explaining these evolutions. It is found that the neutron SO splittings for a given pair of single-particle states are strongly influenced by the single proton on the levels with similar quantum numbers. Due to the isospin factor in the tensor term of the  $\pi$ - $N$  interaction, the neutron-proton tensor force is stronger than the neutron-neutron one. Therefore, the impact of the tensor force on the neutron SO splittings of the neutron drop with  $N = 20$  by adding a proton is more prominent than by adding a neutron. Similar behaviors of the SO splittings have also been found for the neutron-proton drops with 20 protons, where the tensor-force strength  $\lambda$  has to be redetermined by reproducing the differences of the SO splittings at  $N = 20$  and  $N = 28$  in the microscopic RBHF results due to large central densities. To further study the tensor-force effects in the realistic nuclear system, it is suggested that a new covariant density functional, guided by the RBHF calculations on neutron-proton drops, should be built to achieve a better constraint for the strength of the tensor force.

#### ACKNOWLEDGMENTS

This work was partly supported by the National Key R&D Program of China (Contracts No. 2017YFE0116700 and No. 2018YFA0404400), the National Natural Science Foundation of China (Grants No. 11935003, No. 11975031, No. 11875075, and No. 11621131001) and the State Key Laboratory of Nuclear Physics and Technology of Peking University (Grant No. NPT2020ZZ01).

- 
- [1] H. Sagawa and G. Colò, *Prog. Part. Nucl. Phys.* **76**, 76 (2014).
  - [2] S. Shen, H. Liang, J. Meng, P. Ring, and S. Zhang, *Phys. Lett. B* **778**, 344 (2018).
  - [3] S. Shen, H. Liang, W. H. Long, J. Meng, and P. Ring, *Prog. Part. Nucl. Phys.* **109**, 103713 (2019).
  - [4] H. A. Bethe, *Phys. Rev.* **57**, 390 (1940).
  - [5] E. Gerjuoy and J. Schwinger, *Phys. Rev.* **61**, 138 (1942).
  - [6] H. Feshbach and W. Rarita, *Phys. Rev.* **75**, 1384 (1949).
  - [7] G. L. Schrenk and A. N. Mitra, *Phys. Rev. Lett.* **19**, 530 (1967).
  - [8] B. S. Pudliner, V. R. Pandharipande, J. Carlson, S. C. Pieper, and R. B. Wiringa, *Phys. Rev. C* **56**, 1720 (1997).
  - [9] T. Otsuka, T. Suzuki, R. Fujimoto, H. Grawe, and Y. Akaishi, *Phys. Rev. Lett.* **95**, 232502 (2005).
  - [10] C. L. Bai, H. Sagawa, H. Q. Zhang, X. Z. Zhang, G. Colò, and F. R. Xu, *Phys. Lett. B* **675**, 28 (2009).
  - [11] C. L. Bai, H. Q. Zhang, H. Sagawa, X. Z. Zhang, G. Colò, and F. R. Xu, *Phys. Rev. Lett.* **105**, 072501 (2010).
  - [12] J. Meng, *Relativistic Density Functional for Nuclear Structure* (World Scientific, Singapore, 2016).
  - [13] A. Bouyssy, J.-F. Mathiot, N. Van Giai, and S. Marcos, *Phys. Rev. C* **36**, 380 (1987).
  - [14] W.-H. Long, N. Van Giai, and J. Meng, *Phys. Lett. B* **640**, 150 (2006).
  - [15] L. J. Jiang, S. Yang, B. Y. Sun, W. H. Long, and H. Q. Gu, *Phys. Rev. C* **91**, 034326 (2015).
  - [16] Y.-Y. Zong and B.-Y. Sun, *Chin. Phys. C* **42**, 024101 (2018).

- [17] Z. Wang, Q. Zhao, H. Liang, and W. H. Long, *Phys. Rev. C* **98**, 034313 (2018).
- [18] W. H. Long, H. Sagawa, N. V. Giai, and J. Meng, *Phys. Rev. C* **76**, 034314 (2007).
- [19] W. Long, H. Sagawa, J. Meng, and N. Van Giai, *Europhys. Lett.* **82**, 12001 (2008).
- [20] J. J. Li, J. Margueron, W. H. Long, and N. Van Giai, *Phys. Lett. B* **753**, 97 (2016).
- [21] Z.-Z. Li, S.-Y. Chang, Q. Zhao, W.-H. Long, and Y.-F. Niu, *Chin. Phys. C* **43**, 074107 (2019).
- [22] J. Liu, Y. F. Niu, and W. H. Long, *Phys. Lett. B* **806**, 135524 (2020).
- [23] G. A. Lalazissis, S. Karatzikos, M. Serra, T. Otsuka, and P. Ring, *Phys. Rev. C* **80**, 041301(R) (2009).
- [24] A. V. Afanasjev and E. Litvinova, *Phys. Rev. C* **92**, 044317 (2015).
- [25] K. Karakatsanis, G. A. Lalazissis, P. Ring, and E. Litvinova, *Phys. Rev. C* **95**, 034318 (2017).
- [26] B. S. Pudliner, A. Smerzi, J. Carlson, V. R. Pandharipande, S. C. Pieper, and D. G. Ravenhall, *Phys. Rev. Lett.* **76**, 2416 (1996).
- [27] A. Smerzi, D. G. Ravenhall, and V. R. Pandharipande, *Phys. Rev. C* **56**, 2549 (1997).
- [28] M. Kortelainen, J. McDonnell, W. Nazarewicz, E. Olsen, P.-G. Reinhard, J. Sarich, N. Schunck, S. M. Wild, D. Davesne, J. Erler, and A. Pastore, *Phys. Rev. C* **89**, 054314 (2014).
- [29] P. W. Zhao and S. Gandolfi, *Phys. Rev. C* **94**, 041302(R) (2016).
- [30] J. Bonnard, M. Grasso, and D. Lacroix, *Phys. Rev. C* **98**, 034319 (2018).
- [31] F. Pederiva, A. Sarsa, K. E. Schmidt, and S. Fantoni, *Nucl. Phys. A* **742**, 255 (2004).
- [32] S. K. Bogner, R. J. Furnstahl, H. Hergert, M. Kortelainen, P. Maris, M. Stoitsov, and J. P. Vary, *Phys. Rev. C* **84**, 044306 (2011).
- [33] S. Gandolfi, J. Carlson, and S. C. Pieper, *Phys. Rev. Lett.* **106**, 012501 (2011).
- [34] P. Maris, J. P. Vary, S. Gandolfi, J. Carlson, and S. C. Pieper, *Phys. Rev. C* **87**, 054318 (2013).
- [35] H. D. Potter, S. Fischer, P. Maris, J. P. Vary, S. Binder, A. Calci, J. Langhammer, and R. Roth, *Phys. Lett. B* **739**, 445 (2014).
- [36] I. Tews, S. Gandolfi, A. Gezerlis, and A. Schwenk, *Phys. Rev. C* **93**, 024305 (2016).
- [37] S. Shen, H. Liang, J. Meng, P. Ring, and S. Zhang, *Phys. Rev. C* **97**, 054312 (2018).
- [38] S. Shen, J. Hu, H. Liang, J. Meng, P. Ring, and S. Zhang, *Chin. Phys. Lett.* **33**, 102103 (2016).
- [39] S. Shen, H. Liang, J. Meng, P. Ring, and S. Zhang, *Phys. Rev. C* **96**, 014316 (2017).
- [40] S. Wang, H. Tong, P. Zhao, and J. Meng, *Phys. Rev. C* **100**, 064319 (2019).
- [41] S. Shen, G. Colò, and X. Roca-Maza, *Phys. Rev. C* **99**, 034322 (2019).
- [42] W. H. Long, P. Ring, N. V. Giai, and J. Meng, *Phys. Rev. C* **81**, 024308 (2010).